

Cite this: *Mol. Syst. Des. Eng.*, 2020,  
5, 139

# Enumeration of *de novo* inorganic complexes for chemical discovery and machine learning†

Stefan Gugler, Jon Paul Janet and Heather J. Kulik \*

Despite being attractive targets for functional materials, the discovery of transition metal complexes with high-throughput computational screening is challenged by the amount of feasible coordination numbers, spin states, or oxidation states and the potentially large sizes of ligands. To overcome these limitations, we take inspiration from organic chemistry where full enumeration of neutral, closed-shell molecules under the constraint of size has enriched discovery efforts. We design monodentate and bidentate ligands from scratch for the construction of mononuclear, octahedral transition metal complexes with up to 13 heavy atoms (*i.e.*, metal, C, N, O, P, or S). From >11 000 theoretical ligands, we develop a heuristic score for ranking a chemically feasible 2500 ligand subset, only 71 of which were previously included in common organic molecule databases. We characterize the top 20% of scored ligands with density functional theory (DFT) in an octahedral homoleptic ligand database (OHLDB). The OHLDB contains i) the geometry optimized structures of 1250 homoleptic octahedral complexes obtained from the enumerated pool of ligands and an open-shell transition metal ( $M(\text{ii})/M(\text{iii})$ ,  $M = \text{Cr, Mn, Fe, or Co}$ ) and ii) the resulting high-spin/low-spin adiabatic electronic energy differences ( $\Delta E_{\text{H-L}}$ ) obtained with hybrid DFT. Over the OHLDB, we observe structure–property (*i.e.*,  $\Delta E_{\text{H-L}}$ ) relationships different from those expected on the basis of ligand field arguments or from our prior data sets. Finally, we demonstrate how incorporating OHLDB data into artificial neural network (ANN) training improves ANN out-of-sample performance on much larger transition metal complexes.

Received 14th June 2019,  
Accepted 3rd July 2019

DOI: 10.1039/c9me00069k

rsc.li/molecular-engineering

## Design, System, Application

We develop a strategy for octahedral transition metal complex design by enumerating potential ligands from scratch. Such complexes are relevant as molecular sensors and switches that can change their ground state spin in response to light, heat, or other stimuli. They are also models of catalytic active sites. We show how our *de novo* enumeration both produces complexes with novel electronic structure and provides training data that improves the baseline performance of our machine learning models (here, artificial neural networks) in out-of-sample tests.

## 1. Introduction

Computational, first-principles (*i.e.*, with density functional theory, DFT) high-throughput screening<sup>1–7</sup> is an essential com-

plement to experimental<sup>8–10</sup> efforts in the discovery and design of molecules and materials. In recent years, machine learning (ML) property prediction models trained on first-principles simulation data have further accelerated this discovery process<sup>4,11–18</sup> throughout chemistry,<sup>19–24</sup> including for catalysis<sup>15,16,25,26</sup> and materials.<sup>4,27–34</sup> Unique challenges arise in applying these tools to the discovery of open shell transition metal complexes, despite their importance as selective catalysts<sup>35–43</sup> and functional materials (*e.g.*, molecular switches or sensors<sup>44–52</sup>). The theoretical chemical space of inorganic complexes is diverse and relatively unexplored due to the variable spin states, oxidation states, and coordination numbers feasible for each metal. The large sizes of inorganic complexes and limited applicability of more affordable semi-empirical<sup>53</sup> or force field<sup>54,55</sup> methods in open-shell transition metal chemistry also hinders the rapid computational exploration of this space.<sup>28</sup>

To accelerate discovery in open-shell transition metal chemistry, we have developed<sup>4,17,27,28,56,57</sup> ML models for

Department of Chemical Engineering, Massachusetts Institute of Technology, Cambridge, MA 02139, USA. E-mail: hjkulik@mit.edu; Tel: +1 617 253 4584

† Electronic supplementary information (ESI) available: SMILES strings and components of scores for M1, M2, and B4 ligands; details of M1, M2, and B4 ligand scoring along with properties of retained ligands; comparison of ligand scores to properties of ChEMBL, DiRef, and GDB-9 molecules; principal component analysis of OHLDB data and comparison to prior calculations; success rate of DFT calculations; spin-splitting properties of new complexes, including  $M(\text{iii})$  boxplot results; analysis of improvement in out-of-sample CSD ANN performance with retrained ANN (PDF). Geometry optimized structures and properties of OHLDB complexes; geometry optimized structures and properties of 1901 training complexes, geometry optimized structures and properties of 116 CSD test case complexes; ANN predictions on OHLDB structures; ANN predictions on CSD structures before and after retraining; ANN models, ANN models, weights and scaling information before and after retraining (ZIP). See DOI: 10.1039/c9me00069k



predicting quantum mechanical properties (here, computed with DFT), including spin-splitting energies,<sup>17,27,56</sup> redox or ionization potentials,<sup>28,56</sup> metal–ligand bond lengths,<sup>17,28</sup> frontier orbital energies,<sup>4</sup> and reaction energetics.<sup>58</sup> A key outstanding challenge for ML model improvement, especially in inorganic chemistry, is the generation of large data sets. While most organic chemistry ML models have been trained<sup>24,59–65</sup> on large (>100k points) data sets<sup>19,66,67</sup> of molecules consisting of up to 9 heavy (*i.e.*, C, N, O, or F) atoms, the higher computational cost associated with the larger number of electrons and added complexity of open-shell wavefunctions have limited data set sizes for inorganic chemistry.<sup>28</sup> Despite these limitations in data set size, ML models for inorganic chemistry on modest data sets are predictive to 1–3 kcal mol<sup>-1</sup> as judged by test set errors.<sup>17,56</sup> However, limited coverage of the wide range of chemical bonding in transition metal complexes means that ML model prediction error can rise rapidly (to *ca.* 6–10 kcal mol<sup>-1</sup> (ref. 17 and 27)) when applied to complexes dissimilar from training data. Thus, an approach to efficiently increase data set diversity would benefit ML models in inorganic chemistry.

Here, we take inspiration from organic chemistry, where systematic enumeration of small, drug-like molecules<sup>68–73</sup> paved the way for large data sets suitable for ML. However, the enumeration of possible inorganic complexes will necessarily differ from such prior organic enumerations, as the properties that make a molecule a good ligand for an inorganic complex (*e.g.*, an unsaturated atom that can freely complex to a metal) are not the same as the characteristics that define closed-shell organic molecules. To construct such a set we note that, whether through *ad hoc* feature engineering<sup>17</sup> or systematic feature selection,<sup>56</sup> the most predictive and transferable feature sets for open-shell transition metal complex properties emphasize metal-local features. For spin-splitting energetics in particular, we found that the 24 most informative heuristic features obtained from feature selec-

tion<sup>28,56</sup> were primarily (80%) comprised of properties from atoms within two bonds of the metal on the molecular graph. Thus, by selecting small ligands and systematically varying their properties, we expect to capture the most important variations needed to improve coverage for ML model training.

In this work, we enumerate *de novo* octahedral transition metal complex ligands, study properties of homoleptic complexes of these ligands with first-principles DFT simulation, and demonstrate the improvement of our inorganic ML models through the inclusion of this data. The rest of this work is as follows. In section 2, we describe our rules for enumerating monodentate and bidentate ligands composed of up to two and four heavy atoms, respectively. In section 3, we describe the Computational details of our simulation methodology. In section 4, we analyze the results of DFT geometry optimizations of homoleptic octahedral complexes built from these ligands and demonstrate how these data points improve ML model performance. Finally, in section 5, we provide our outlook and conclusions.

## 2. Enumerating inorganic complex ligands

We enumerated candidate ligands from the elements C, N, O, P, or S, which were chosen i) for their abundance<sup>70,71,74</sup> on earth and in organisms and ii) to enable comparison between isovalent compounds (*i.e.*, N *vs.* P and O *vs.* S). Molecules were classified into three ligand types defined by the number of heavy (*i.e.*, non-H) atoms: monodentate ligands with one (M1) or two (M2) heavy atoms and bidentate ligands with four heavy atoms (B4) created from joining two identical M2 heavy atom pairs, all of which were variably passivated with H atoms (Fig. 1). After enumeration of all theoretical ligands of these three types, we carried out two filtering steps, first excluding major violations of chemical bonding rules, then scoring the remaining cases and retaining the top-scoring ligands (Fig. 1). We penalized but did not exclude ligands that do not have octet valence or neutral charge, diverging from previous organic enumeration efforts<sup>69</sup> that were not focused on ligand generation for inorganic chemistry. We did however remove any enumerated ligands with an odd number of electrons to avoid ligand noninnocence.<sup>75</sup> Ligand scores were based on heuristic properties, *i.e.*: i) the number of H atoms bonded to any of the heavy atoms, *h*; ii) the charge, *c*; iii) the number of lone pairs, *l*; and iv) the number of valence electrons, *v*, as described next.

### 2.1. M1 ligands

The simplest case corresponds to M1 ligands generated from a single heavy (*i.e.*, C, N, O, P, S) atom with variable H atom passivation and charge. For initial enumeration, there were 5 possible heavy elements, we permitted 5 overall charge values, *c*, from -2 to 2 in an increment of 1, and we varied the number of H atoms added, *h*, over the range of 0 to 4. This combination produced  $5 \times 5 \times 5 = 125$  theoretical M1



Heather J. Kulik

*Heather J. Kulik is an Associate Professor in Chemical Engineering at MIT. She received her B.E. in Chemical Engineering from Cooper Union in 2004 and Ph.D. in Materials Science and Engineering from MIT in 2009. Following postdocs at Lawrence Livermore and Stanford, she returned to MIT. Her work has been recognized by a Burroughs Wellcome Fund Career Award at the Scientific Interface, Office of Naval Research Young Investiga-*

*tor Award, DARPA Young Faculty Award, AAAS Marion Milligan Mason Award, NSF CAREER, the ACS OpenEye Award for Outstanding Junior Faculty in Computational Chemistry, and a Journal of Physical Chemistry Lectureship, among others.*



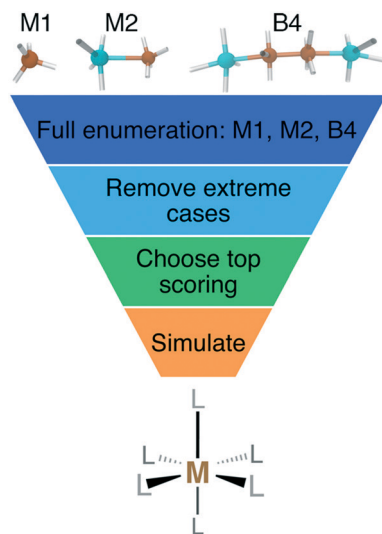


**Fig. 1** Schematic of M1, M2, and B4 ligands, as designated by the number of heavy atoms (*i.e.*, C, N, O, P, or S) and number of metal-coordinating atoms (top) with hypothetical places to add hydrogen atoms indicated with white sticks. The filtering process consists first of enumeration of all possible ligands, removal of extreme cases, scoring and retaining top-scoring ligands, and then finally the simulation of homoleptic  $M(II)/M(III)$  ( $M = Cr, Mn, Fe, \text{ or } Co$ ) octahedral complexes with DFT as indicated in the flowchart.

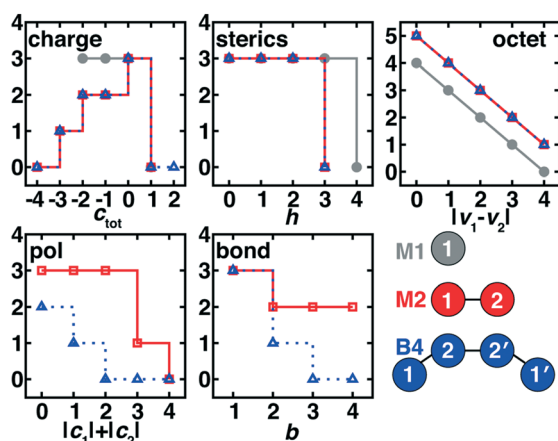


**Fig. 2** Scores for each of the three ligand types (*i.e.*, M1 in gray circles and solid lines, M2 in red squares and solid lines, and B4 in blue triangles and dotted lines) colored according to the bottom right inset. Three of the scores apply to all three ligand types: charge ( $c_{tot}$ , top left); sterics, as judged through number of hydrogen atoms on the metal-coordinating atom ( $h$ , top middle); and octet, as judged through valence deviations ( $|v_1 - v_2|$ , where  $v_2 = 8$  for M1 ligands, top right). Two of the scores apply only to M2 and B4 ligands: pol, the polarization measured by  $|c_1| + |c_2|$  (bottom, left) and bond,  $b$ , for the 1–2 bond order (bottom, middle).

ligands. After discarding ligands with an odd number of electrons and strongly positively charged ligands (*i.e.*, retaining only  $-2 \leq c \leq 1$ ), we obtained 50 ligands for the second filtering step.

For M1 ligands, we assigned three scores,  $s$ , for the charge ( $s_{charge}$ ), sterics (*i.e.*, presence of H atoms,  $s_{sterics}$ ), and accordance with the octet rule ( $s_{octet}$ ). We favored neutral and weakly negative ligands ( $s_{charge} = 3$  for  $-2 \leq c \leq 0$ ) over posi-

tively charged ligands ( $s_{charge} = 0$  for  $c = 1$ ), due to the fact that ligands will be complexed with positively charged metal centers (Fig. 2). We penalized  $h = 4$  ( $s_{sterics} = 0$ ) passivation over all other choices ( $s_{sterics} = 3$ ) because large numbers of H atoms hinder the heavy atom from coordinating to the metal center (Fig. 2). We reduced the  $s_{octet}$  of a valence,  $v$ , in proportion to its violation of the octet rule (Fig. 2):

$$s_{octet} = 4 - |8 - v| \quad (1)$$

A total score,  $s_{tot}$ , for M1 ligands was given by:

$$s_{tot} = s_{charge} + s_{sterics} + s_{octet} \quad (2)$$

which theoretically ranged from 0 to 10. In practice, over the 50 pre-filtered ligands, the scores ranged from 3 to 10.

Common M1-type ligands in the spectrochemical series<sup>76</sup> include  $\text{OH}^-$ ,  $\text{H}_2\text{O}$ , and  $\text{NH}_3$ , all of which were top scoring (*i.e.*,  $s_{tot} = 10$ , Fig. 3 and ESI† Table S1). M1 ligands with  $s_{tot} = 8$  that have been observed experimentally or invoked in the spectrochemical series include methylene<sup>77</sup> ( $\text{CH}_2$ ) and elemental sulfur<sup>78</sup> (Fig. 3). Still lower scores (*i.e.*,  $s_{tot} = 7$ ) arose primarily due to penalties for: i) steric repulsion, as in methane ( $\text{CH}_4$ ) or ii) charge, as in sulfonium ( $\text{SH}_3^+$ ) and hydronium ( $\text{OH}_3^+$ ) (Fig. 3). The lowest scoring ligand ( $s_{tot} = 3$ ),  $\text{OH}_4^{2-}$ , simultaneously violates steric and octet rules (Fig. 3). After filtering on score, we retained only the 29 M1 ligands with  $s_{tot} \geq 8$ , all of which were neutral (9) or negatively charged (20, see ESI† Fig. S1).

## 2.2. M2 ligands

For initial enumeration of M2 ligands, two atoms of the 5 possible heavy elements were joined, the total charge was constrained overall (*i.e.*, retaining only  $-4 \leq c_{tot} \leq 4$ ), and each atom was allowed to have between 0 and 4 passivating H atoms. The identities of the first and second atoms (*i.e.*,

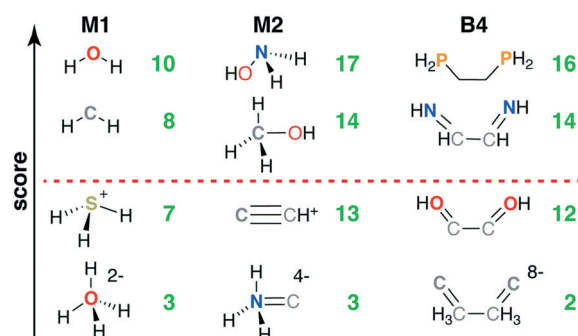


**Fig. 3** Four representative structures of M1 (left), M2 (middle), and B4 (right) ligand types ordered by their relative scores from top to bottom as indicated by left axis. The topmost and bottommost structures in each case correspond to ligands that score the maximum and minimum observed scores. The quantitative total scores for the respective ligand types are shown in each case at right in green, and the red dashed line indicates the separation between retained ligands and those below their respective ligand type cutoffs.



indexed 1 and 2) were treated distinguishably because we defined the first atom as coordinating the metal, and we allowed the charges and passivating H atoms to vary between the two atoms. Thus, the initial theoretical space of M2 ligands was 5625, from 25 combinations of five types of atom 1 and 2 elements, 9 charge assignments, and 25 combinations of atom 1 and atom 2 H-atom passivation.

In addition to eliminating ligands that produce odd numbers of electrons as in the M1 ligands, we also considered the expected bonding between the two heavy atoms in the ligand for filtering and scoring of the M2 ligands. To determine M2 candidate ligand bond order, we first assigned individual  $c_1$ ,  $c_2$  charges by choosing from all combinations that could produce the  $c_{\text{tot}}$  value under constraint that the valence,  $\nu$ , of each  $i$ th atom was satisfied:

$$\nu_i = \nu_i - c_i - 2l_i - h_i \quad (3)$$

where  $l_i$  are the number of lone pairs of the atom (e.g., 1 for N atom),  $h_i$  are the number of hydrogen atoms, and  $\nu_i$  are the maximum standard valence electrons (e.g., 5 for N atom, see ESI† Table S2). From all possible values of  $c_1$  and  $c_2$  that satisfy eqn (3), we chose the values that minimized  $|\nu_1 - \nu_2|$ . The bond order,  $b$ , was then assigned as:

$$b = \min(\nu_1, \nu_2) \quad (4)$$

with an allowable range of  $0 < b \leq 4$ , and  $b$  was set to 0 if eqn (3) could not be satisfied (ESI† Algorithm S1). For example,  $c_{\text{tot}} = 1$  for the molecule  $\text{NO}^+$  could be distributed as  $c_i = +2/-1$  or  $c_i = +1/0$ ; the algorithm selected  $c_{\text{N}} = +1$  and  $c_{\text{O}} = 0$  because this result gives  $\nu_1 = \nu_2 = 2$  to minimize  $|\nu_1 - \nu_2|$  and thus maximize  $b$  (ESI† Algorithm S1).

After assembling these M2 ligands, we discarded i) highly positively charged ligands (i.e.,  $c_{\text{tot}} > 1$ ), ii) metal-coordinating heavy atoms (i.e., atom 1) with  $h > 3$ , and iii) ligands with  $b = 0$  predicted between the two heavy atoms. We then scored the remaining 1171 ligands with scores adapted and augmented from the M1 case. In comparison to M1 charge scoring, the M2 ligand charge score was biased toward neutral ligands ( $s_{\text{charge}} = 3$  for  $c_{\text{tot}} = 0$ ) and weakly penalized intermediate, negatively charged ligands ( $s_{\text{charge}} = 2$  for  $c_{\text{tot}} = -1$  or  $-2$ ,  $s_{\text{charge}} = 1$  for  $c_{\text{tot}} = -3$ , see Fig. 2). Sterics of the M2 ligand were scored only for the metal-coordinating atom, but we penalized  $h = 3$  or higher due to the presence of the second heavy atom (i.e.,  $s_{\text{sterics}} = 3$  for  $h < 3$ , Fig. 2). The M2  $s_{\text{octet}}$  score was applied over atom 1 and 2  $\nu$  values (Fig. 2):

$$s_{\text{octet}} = 5 - |\nu_1 - \nu_2| \quad (5)$$

where the absolute difference of  $\nu_1$  and  $\nu_2$  ranged from 0 to 4 over the retained ligands. This produced a practical  $s_{\text{octet}}$  of 1 to 5 (Fig. 2 and see ESI†).

We introduced two bond-specific scores for the bond between the two heavy atoms in the M2 ligands: i) bond order,  $s_{\text{bond}}$  and ii) charge polarization,  $s_{\text{pol}}$ . We already excluded

$b = 0$  molecules, but in scoring we favored  $b = 1$  ( $s_{\text{bond}} = 3$ ) weakly over  $b > 1$  ( $s_{\text{bond}} = 2$ ) to avoid oversampling high bond-order, few-atom M2 ligands (Fig. 2). We disfavored unphysically ionic bonds in the present ligands by scoring highest the cases with low atom-wise charge assignment ( $s_{\text{pol}} = 3$  for  $|c_1| + |c_2| \leq 2$ ), assigning intermediate scores for moderate polarization ( $s_{\text{pol}} = 1$  for  $|c_1| + |c_2| = 3$ ) and penalizing the highest formal charges ( $s_{\text{pol}} = 0$  for  $|c_1| + |c_2| = 4$ , see Fig. 2). A total M2 ligand score was thus:

$$s_{\text{tot}} = s_{\text{charge}} + s_{\text{sterics}} + s_{\text{octet}} + s_{\text{bond}} + s_{\text{pol}} \quad (6)$$

which had a range of 3 to 17 over scored ligands, due to minimum values for  $s_{\text{octet}}$  of 1 and  $s_{\text{bond}}$  of 2 (Fig. 2 and ESI† Table S3).

The 55 highest scoring ligands ( $s_{\text{tot}} = 17$ ) include the common metal-complexing ligands methylamine ( $\text{NH}_2\text{CH}_3$ ),<sup>79</sup> hydrogen peroxide ( $\text{H}_2\text{O}_2$ ), and both hydroxylamine ( $\text{NH}_2\text{OH}$ )<sup>80</sup> and its experimentally-observed analogue, thiophosphinous acid<sup>81</sup> ( $\text{PH}_2\text{SH}$ , Fig. 3). Both reactive peroxide<sup>82</sup> ( $\text{O}_2^{2-}$ ) and nitrosyl<sup>83</sup> ( $\text{NO}^-$ ) ( $s_{\text{tot}} = 15$ ) score highly as do stable small molecules such as  $\text{N}_2$  and  $\text{HCN}$  ( $s_{\text{tot}} = 16$ ) and methanol ( $\text{CH}_3\text{OH}$ ) (O-coordinating  $s_{\text{tot}} = 17$ , C-coordinating  $s_{\text{tot}} = 14$ , see Fig. 3). Most M2-type ligands in the spectrochemical series<sup>84</sup> have high scores (e.g.,  $\text{CN}^-$ ,  $s_{\text{tot}} = 15$  and  $\text{CO}$ ,  $s_{\text{tot}} = 16$ ), with  $\text{NO}^+$  ( $s_{\text{tot}} = 13$ ) scoring the lowest due to its positive charge. Other  $s_{\text{tot}} = 13$  ligands include sterically hindered ligands (e.g.,  $\text{NH}_3\text{NH}_3^{2-}$ ) or likely unstable, positively charged species, such as  $\text{CCH}^+$  (Fig. 3). The lowest score ( $s_{\text{tot}} = 3$ ) was only assigned to 2 ligands when steric repulsion, octet rule violation, and unfavorable charges were all present in a single molecule (e.g.,  $\text{NH}_3\text{C}^{4-}$ :  $s_{\text{octet}} = 1$ ,  $s_{\text{bond}} = 2$ , all other scores are zero, see Fig. 3). From the scored subset of M2 ligands, we therefore retained the 494 M2 ligands with  $s_{\text{tot}} \geq 14$  for further characterization with DFT (sec. 4). Most of the retained ligands have single or double bonds between the two heavy atoms and are neutral or negatively charged (ESI† Fig. S2).

### 2.3. B4 ligands

We generated symmetric bidentate B4 ligands solely by joining two identical M2 ligands from the original pool of 5625 theoretical M2 ligands, and so there were also 5625 theoretical B4 ligands. To simplify our algorithmic approach, we did not remove hydrogen atoms or use fragments with unpaired electrons to generate B4 ligands, as might be done in an intuitive dimerization procedure. If an atom was labeled as the metal-coordinating atom (i.e., 1) in the M2 ligand, it remained so in the B4 ligands, and the identical atoms in the ligand were assigned the indices 1' and 2'. To construct the B4 ligands from the M2 substituents, we defined the 2-2' bond order ( $b_{2-2'}$ ) by reassigning the value for  $b_{1-2}$  (and equivalently  $b_{1'-2'}$ , Fig. 2). This reassignment was necessary because the number of electrons and hydrogen atoms in the B4 ligand is simply twice that of the original M2 ligand. To



determine the reassigned bond orders, we took the  $c_{\text{tot}}$  from the parent M2 molecule and computed all possible  $c_i$  and  $\nu_i$ , requiring that  $\nu_1 > 0$  and  $\nu_2 > 1$ , where  $\nu_i$  was assigned from eqn (3).

We next determined the  $b_{1-2}$  and  $b_{2-2'}$  bond orders simultaneously by iterating over allowed values between single and triple bonds:

$$\{b_{1-2}, b_{2-2'}\} = \underset{\substack{b_{1-2} \in \{1,2,3\} \\ b_{2-2'} \in \{1,2,3\}}}{\text{argmin}} \left\{ |\nu_1 - b_{1-2}| + |\nu_2 - b_{1-2} - b_{2-2'}| \right\} \quad (7)$$

where the first term is the difference between atom 1 valence electrons and the number of electrons used in the 1–2 bond, and the second term is the difference between the atom 2 valence electrons and those used in either the 1–2 or 2–2' bond (ESI† Algorithm S2). If multiple choices of  $b_{1-2}$  and  $b_{2-2'}$  minimized the argument, we selected the one with lower charge polarization (*i.e.*, lower  $|c_1| + |c_2|$ ), and zero bond order was again assigned if no result satisfied the equation (ESI† Algorithm S2). For example, the neutral M2 ligand  $\text{NH}_2=\text{CH}$  has  $b_{1-2} = 2$  with  $c_1 = -1$  and  $c_2 = 1$ . The resulting B4 ligand formed from two of these M2 ligands is  $\text{NH}_2-\text{CH}=\text{CH}-\text{NH}_2$ , which has the same net charge but neutral atom-wise charge assignments with  $b_{1-2} = b_{1'-2'} = 1$  and  $b_{2-2'} = 2$ .

After assembling all theoretical B4 ligands, we discarded i) ligands with two consecutive double bonds or any cases with triple bonds that would be unable to form a 1–2–2'–1' dihedral necessary to enable bidentate metal coordination, ii) strongly charged ligands with total charge (*i.e.*, twice the charge of the original M2 ligand) higher than 4 or more negative than –8, iii) cases in which any bond orders were assigned to be zero, and iv) ligands with connecting atoms that had three or more passivating hydrogen atoms. These down-selection steps left a pool of 1356 B4 ligands suitable for further scoring with a five-component score similar to that applied to the M2 ligands. Both  $s_{\text{charge}}$  and  $s_{\text{sterics}}$  were unchanged from the M2 case but were evaluated, respectively, on the charge only of the original M2 fragment (*i.e.*, half of the total B4 ligand charge) or a single relevant connecting atom (Fig. 2). The B4  $s_{\text{octet}}$  was also scored only for a single building block using eqn (5) but using the revised valency after charge redistribution (Fig. 2). After redistribution of charges, we scored a single 1–2 pair, penalizing strong polarization ( $s_{\text{pol}} = 0$  for  $|c_1| + |c_2| > 1$ ), favoring completely neutral atomic charges ( $s_{\text{pol}} = 2$  for  $|c_1| + |c_2| = 0$ ), and assigning an intermediate score ( $s_{\text{pol}} = 1$ ) for slight polarization (*i.e.*,  $|c_1| + |c_2| = 1$ , see Fig. 2). We also computed  $s_{\text{bond}}$  only on the 1–2 bond and reduced it with respect to M2 scoring for higher bond orders ( $s_{\text{bond}} = 3$  for  $b = 1$ ,  $s_{\text{bond}} = 1$  for  $b = 2$ , see Fig. 2).

The five B4 metrics were combined as in eqn (6) for a total score with a range of 2 to 16 across ligands retained for scoring (Fig. 1). Ethylenediamine (en,  $\text{C}_2\text{H}_8\text{N}_2$ ) is the only B4-type ligand in the spectrochemical series,<sup>84</sup> and it has a maximum score ( $s_{\text{tot}} = 16$ ) as does its phosphorus analogue, 1,2-

ethanediyldiphosphine ( $\text{C}_2\text{H}_8\text{P}_2$ ,  $s_{\text{tot}} = 16$ , Fig. 3 and ESI† Table S4). Other common ligands that score highly include ethylene glycol ( $\text{C}_2\text{H}_6\text{O}_2$ ,  $s_{\text{tot}} = 16$ ) and 1,2-ethanediiimine ( $\text{C}_2\text{H}_4\text{N}_2$ ,  $s_{\text{tot}} = 14$ ), which contains a bonding pattern analogous to that observed in the common bipyridine ligand (Fig. 3). Stable organic molecules that are sterically hindered and would make poor ligands, *e.g.*, butane ( $\text{C}_4\text{H}_{10}$ ,  $s_{\text{tot}} = 13$ ), score more poorly than unstable but likely metal-coordinating molecules, *e.g.*, tetraoxidane<sup>85</sup> ( $\text{H}_2\text{O}_4$ ,  $s_{\text{tot}} = 16$ , Fig. 3). Other molecules with intermediate scores ( $s_{\text{tot}} = 12$ ) typically score lower due to a combination of steric hindrance, charge, and violations of the octet rule (*e.g.*,  $\text{S}_4$ , or  $\text{HOC}_2\text{OH}$ , Fig. 3). The lowest scoring ligands are charged, have polarized bonds, and are octet violating (*e.g.*,  $\text{CCH}_3\text{CH}_3\text{C}^{8-}$ ,  $s_{\text{tot}} = 2$ , Fig. 3). Following these holistic observations, we retained only the 47 B4 ligands with  $s_{\text{tot}} \geq 14$  for subsequent DFT calculations (ESI† Fig. S3).

#### 2.4. Overall ligand analysis

From an original combinatorial space of 11 325 theoretical M1, M2, and B4 ligands, we scored 2577 ligands and identified the top 20% (570 ligands) as good candidates for DFT characterization (Fig. 1 and see sec. 4). The other 8748 ligands were eliminated prior to scoring due to disqualifications ranging from unpaired electrons on the ligand, zero bond order between heavy atoms or unsuitable bond order for bidentate coordination, high net positive charge that would prevent coordinating a positively charged metal, or strong steric repulsion from a high number of hydrogen atoms on the metal-coordinating atom that would prevent metal coordination. All such excluded ligands are provided in the ESI† and can be interpreted as scoring zero in comparison to the retained ligands that all score higher. We next compared characteristics of these ligands to molecules in other curated data sets that satisfy M1, M2, or B4 ligand definitions. We focused on three representative databases: ChEMBL,<sup>86</sup> the generated database of enumerated organic molecules with up to 9 heavy atoms, GDB-9;<sup>69</sup> and a database of experimentally and computationally characterized diatomic molecules, DiRef.<sup>87</sup> Across these databases, 71 of the 2577 ligands were observed in at least one database, 17 occurred in more than one database, and most are diatomic molecules found only in DiRef<sup>87</sup> (ESI† Table S5). The majority (55) of database ligands are M2 type, and 46 of these M2-type molecules are present twice in the enumerated ligand set, distinguished only by the metal coordinating atom and corresponding to a single chemical species. Thus, the 71 ligands identified in existing databases (DBs) are 48 chemically distinct species (ESI† Table S5).

To simplify comparison of scores across the three ligand types, we obtained scaled scores,  $s_{\text{scaled}}$ , between the minimum and maximum observed  $s_{\text{tot}}$  values within each ligand type:

$$s_{\text{scaled}} = \frac{s_{\text{tot}} - s_{\text{tot}}^{\text{min}}}{s_{\text{tot}}^{\text{max}} - s_{\text{tot}}^{\text{min}}} \times 100 \quad (8)$$



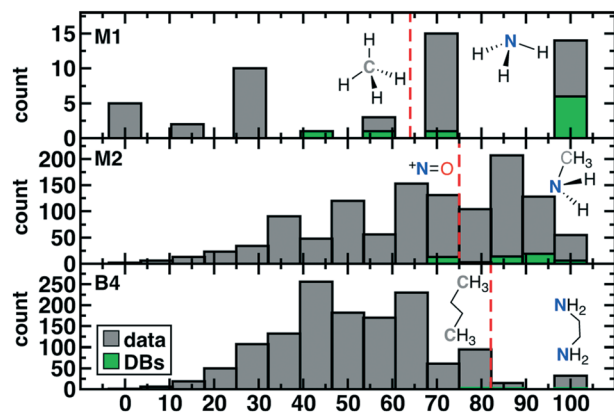


Fig. 4 Distribution of scaled scores for 50 M1 (top), 1171 M2 (middle), and 1356 B4 (bottom) ligands over all data described in this work (bars shown in gray) as well as 71 ligands from three databases (DBs, in green). Representative molecules above and below the cutoff for ligand retention (red vertical dashed line) are shown in inset with the metal-coordinating atom in bold.

The scaled threshold for retention is lowest for M1 ligands (>71%) and highest for the B4 cases (>86%, see Fig. 4). Over all ligands, 75% (53 of 71 overall; 36 of 48 unique) of compounds found in DBs were above the relevant ligand cutoff (Fig. 4). The majority (13 of 18, 7 of 12 unique) of below-cutoff ligands are M2 type and correspond to positively charged diatomics from DiRef<sup>67</sup> (e.g.,  $\text{NO}^+$  and  $\text{PS}^+$  ESI<sup>†</sup> Table S5). Although such ligands are relevant for heteroleptic transition metal complexes, our focus on homoleptic octahedral complexes with high valent metals motivated penalizing positively charged ligands (see Fig. 2). Our restriction to octahedral complexes is motivated by their relevance in catalysis and functional materials, but study of heteroleptic or lower coordination number complexes in future work will motivate alternate scoring. The remaining database ligands below threshold typically exhibit steric hindrance (e.g., M1:  $\text{CH}_4$  or B4:  $\text{C}_2\text{H}_{10}$ , see Fig. 4). Conversely, known good inorganic ligands such as M1 ammonia, M2 methylamine, or B4 ethylenediamine are all among the top scoring database ligands (Fig. 4 and ESI<sup>†</sup> Table S5).

Overall, the enumeration recovered small molecules previously observed in other databases that are likely ligands in inorganic chemistry. Beyond validation of scoring heuristics, the large number of enumerated and retained ligands not present in other databases (i.e., around 90% or 517 of 570) suggests that our data set contains unique chemical bonding configurations. Thus, it will be useful to identify through first-principles DFT simulation the extent to which complexes could be formed from these ligands.

### 3. Computational details

Homoleptic, mononuclear octahedral transition metal complexes were generated from *de novo* ligands (sec. 2) with the molSimplify<sup>3</sup> toolkit and molSimplify Automatic Design (mAD),<sup>4,27</sup> which automated both structure and input file

generation. The molSimplify<sup>3</sup> code uses OpenBabel<sup>5,88</sup> as a backend for force field-based transition metal complex preoptimization prior to first-principles simulation with DFT. DFT geometry optimizations were carried out using TeraChem<sup>89,90</sup> using the B3LYP<sup>91–93</sup> hybrid DFT functional. The default definition of B3LYP in TeraChem employs the VWN1-RPA<sup>94</sup> form for the local density approximation correlation component. The LANL2DZ<sup>95</sup> effective core potential was employed for transition metals with the 6-31G\* basis for all other atoms. These choices were made due to the limited effect of a modest basis set on the relative energies of interest<sup>96</sup> and to enable comparison to previously generated data sets.<sup>17,27,56</sup>

All complexes were generated with four metals ( $M = \text{Cr}$ ,  $\text{Mn}$ ,  $\text{Fe}$ , and  $\text{Co}$ ) in  $M(\text{II})$  and  $M(\text{III})$  oxidation states. The differences between high (H) and low (L) spin states,  $\Delta E_{\text{H-L}}$ , was computed as the electronic energy difference between the two geometry-optimized states (i.e., the adiabatic energy difference). This choice is motivated by the fact that spin-state change is slower than other processes (e.g., optical excitations) for which a vertical energy evaluation may be more appropriate. The high-spin/low-spin definitions for the metals studied in this work are: quintet-singlet for  $d^6$   $\text{Co}(\text{III})/\text{Fe}(\text{II})$ , sextet-doublet for  $d^5$   $\text{Fe}(\text{III})/\text{Mn}(\text{II})$ , quintet-singlet for  $d^4$   $\text{Mn}(\text{III})/\text{Cr}(\text{II})$ , and quartet-doublet for both  $d^3$   $\text{Cr}(\text{III})$  and  $d^7$   $\text{Co}(\text{II})$ . Although thermodynamic and solvent corrections are known to be important in making direct comparison with experimental spin state ordering,<sup>97</sup> the two corrections typically have compensating effects,<sup>96,97</sup> and we therefore focused on relationships between ligand identity and DFT adiabatic, electronic  $\Delta E_{\text{H-L}}$  energies. All open-shell calculations (i.e., non-singlet spin states) were carried out with level shifting<sup>98</sup> using spin-up and spin-down level shifts of 1.0 and 0.1 Ha, respectively. Geometry optimizations used the L-BFGS algorithm in translation rotation internal coordinates (TRIC)<sup>99</sup> as implemented in TeraChem to the default tolerances of  $4.5 \times 10^{-4}$  Hartree/Bohr for the maximum gradient and  $1 \times 10^{-6}$  Hartree for the change in energy between steps.

### 4. Properties of *de novo* transition metal complexes

We next computed with DFT properties of homoleptic octahedral transition metal complexes containing the curated *de novo* ligands. Here, we focus on the high-spin to low-spin adiabatic energy splitting,  $\Delta E_{\text{H-L}}$ , of  $M(\text{II})$  and  $M(\text{III})$  ( $M = \text{Cr}$ ,  $\text{Mn}$ ,  $\text{Fe}$ , or  $\text{Co}$ ) complexes, which we obtained with hybrid DFT for comparison to both prior DFT results and ML models<sup>17,27,56</sup> (see sec. 3). Although quantitative spin-state assignment remains an outstanding challenge for DFT,<sup>97,100–106</sup> with no one-size-fits-all functional for spin-state energetics motivating more advanced methods,<sup>107–109</sup> ligand-dependent trends in relative spin-state ordering are expected to be less sensitive to method choice. From the 570 high-scoring ligands in sec. 2, we excluded 10 M1 and 164 M2 ligands with net  $-2$  charge from calculation due to the high, negative complex charge







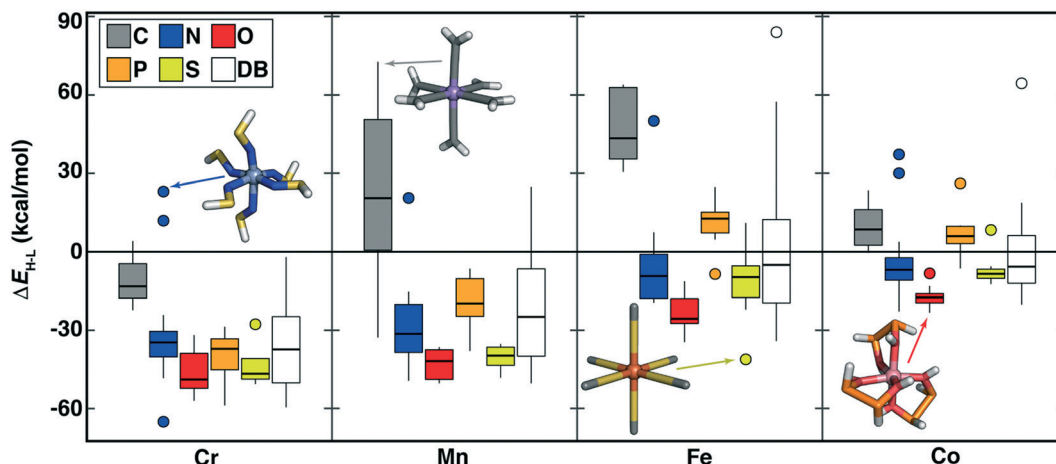


Fig. 7 Boxplots of  $M(\text{II})$  ( $M = \text{Cr}, \text{Mn}, \text{Fe}, \text{or Co}$ )  $\Delta E_{\text{H-L}}$  (in  $\text{kcal mol}^{-1}$ ) for ligands grouped by metal and by ligand-coordinating-atom (C in gray, N in blue, O in red, P in orange, and S in yellow, as shown in inset legend). Each box indicates the median by a horizontal line, the interquartile range (IQR), and whiskers indicate  $1.5 \times$  the IQR. Here, DB (white boxplot) corresponds to range of  $\Delta E_{\text{H-L}}$  values from prior work in ref. 4 and 56 for the relevant metal, regardless of coordinating atom.

Unsaturated carbon-coordinating ligands (*e.g.*,  $\text{CCH}_2$  in  $\text{Mn}(\text{II})(\text{CCH}_2)_6$   $\Delta E_{\text{H-L}} = 72.6 \text{ kcal mol}^{-1}$ ) are known to be low-spin directing ligands but most were absent from our earlier data set, as were more unusual low-spin-directing ligands such as  $\text{CHOH}$  or  $\text{CHNH}_2$  ( $\text{Mn}(\text{II})$   $\Delta E_{\text{H-L}} = 47$  to  $62 \text{ kcal mol}^{-1}$ , Fig. 7). The sulfur-coordinated  $\text{Fe}(\text{II})$  complexes in our new data set span from low-spin (*e.g.*, monodentate  $\text{SHOH}$ :  $\Delta E_{\text{H-L}} = 11.0 \text{ kcal mol}^{-1}$  or bidentate  $\text{SC}_2\text{H}_2\text{S}$ :  $\Delta E_{\text{H-L}} = 10.3 \text{ kcal mol}^{-1}$ ) to high-spin (*e.g.*,  $\text{SC}$ :  $\Delta E_{\text{H-L}} = -41.1 \text{ kcal mol}^{-1}$ ), corresponding to a range that we had not observed in prior  $\text{Fe}(\text{II})$  data (Fig. 7). Since sulfur is considered a soft element, low-spin sulfur complexes are somewhat surprising. Examination of the OHLDB confirms that the bidentate  $\text{SC}_2\text{H}_2\text{S}$  ligand also forms low-spin

complexes with  $\text{Fe}(\text{III})$  and  $\text{Co}(\text{II/III})$  but forms high-spin complexes with  $\text{Cr}(\text{II})$  and  $\text{Mn}(\text{III})$  (see ESI<sup>†</sup>). Saturating the sulfur (*i.e.*,  $\text{SHC}_2\text{H}_2\text{SH}$ ) and the carbon backbone (*i.e.*,  $\text{SHC}_2\text{H}_4\text{SH}$ ) instead yields the expected, uniformly high-spin complexes regardless of metal center and oxidation state (see ESI<sup>†</sup>). Although oxygen-coordinating ligands are known to be weak-field, high-spin directing in nature, diverse ligand chemistry in the OHLDB yields, in addition to those previously observed, unexpectedly high-spin complexes *e.g.*,  $\text{Co}(\text{II})(\text{OHP}_2\text{-H}_2\text{OH})_3$  ( $\Delta E_{\text{H-L}} = -22.8 \text{ kcal mol}^{-1}$ , Fig. 7). This bidentate ligand and the isoelectronic  $\text{OHS}_2\text{OH}$  ligand produce among the most high-spin-favoring  $\text{Cr}(\text{II})/\text{O}$ -coordinating complexes ( $\Delta E_{\text{H-L}}$  *ca.*  $-49$  to  $-52 \text{ kcal mol}^{-1}$ , see ESI<sup>†</sup>).

The OHLDB also enables examination of how isoivalent and isoelectronic variations in ligands alter spin-state ordering (Fig. 8). Here, we focus on the widely-studied  $\text{CO}$  ligand and related isoivalent and isoelectronic species, including those in the spectrochemical series<sup>76</sup> (*e.g.*,  $\text{CN}^-$ ) and other common molecules (*e.g.*,  $\text{HCN}$  and  $\text{N}_2$ , Fig. 8). Given ligand definitions,  $\Delta E_{\text{H-L}}$  can in principle be obtained for either orientation of asymmetric  $\text{M}_2$  ligands, but only 14 of these ligands in practice yielded at least one  $\Delta E_{\text{H-L}}$  value for any metal or oxidation state (Fig. 8). High-spin  $\text{Fe}(\text{II})$  or  $\text{Fe}(\text{III})$  complexes are formed from either homonuclear ligands (*e.g.*,  $\text{N}_2$  and  $\text{P}_2$ ) or cases where the weaker-field element coordinates the metal (*e.g.*,  $\text{SC}$ ,  $\text{OC}$ ), despite being isoivalent or isoelectronic with low-spin directing  $\text{CO}$  (Fig. 8). These effects are not additive by element, where the  $\text{NP}$  ligand is low-spin directing, in spite of the high spin preferences of  $\text{N}_2$  and  $\text{P}_2$  (Fig. 8). Although  $\text{CO}$  is often invoked as one of the strongest field ligands ( $\Delta E_{\text{H-L}} = 20$ – $30 \text{ kcal mol}^{-1}$  for  $\text{Fe}(\text{II})$  or  $\text{Fe}(\text{III})$  complexes), five ligands form even more low-spin-favoring complexes, including those where  $\text{O}$  is replaced by anionic (*e.g.*,  $\text{CN}^-$ ,  $\text{CP}^-$ ) or less electron withdrawing species (*e.g.*,  $\text{CCH}^-$ ,  $\text{CNH}$ , or  $\text{CS}$ , Fig. 8). The trends observed for iron complexes generally hold for other metals, with  $\text{Co}(\text{III})$  complexes

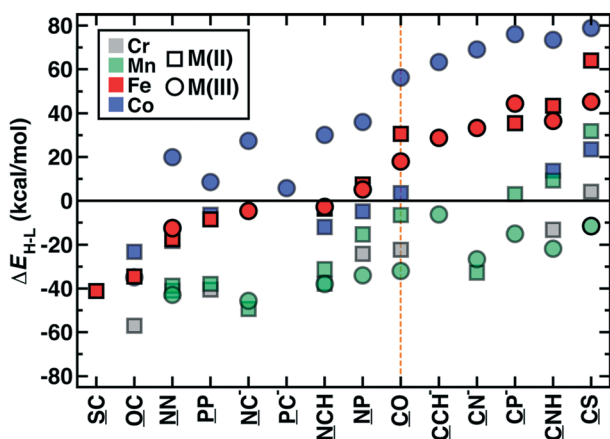


Fig. 8 Adiabatic gas phase spin splitting,  $\Delta E_{\text{H-L}}$ , in  $\text{kcal mol}^{-1}$  for octahedral complexes with  $\text{CO}$  and isoivalent or isoelectronic ligands. Complex energetics are shown for all converged DFT results in  $M(\text{II})$  (squares) and  $M(\text{III})$  (circles) oxidation states with  $\text{Cr}$  (gray),  $\text{Mn}$  (green),  $\text{Fe}$  (red), and  $\text{Co}$  (blue) metals. Ligands are ordered to be monotonically increasing for  $\text{Fe}(\text{II/III})$  complexes, which are shown as solid red symbols, whereas all other metals and oxidation states are shown as translucent symbols to aid comparison. The metal coordinating atom in the ligand is underlined.





18-1-2434 and a 2017 MIT Energy Initiative seed grant. H. J. K. holds a Career Award at the Scientific Interface from the Burroughs Wellcome Fund. This work was supported in part by an AAAS Marion Milligan Mason award (to H. J. K.). This work was carried out in part using computational resources from the Extreme Science and Engineering Discovery Environment (XSEDE), which is supported by National Science Foundation grant number ACI-1548562. This work used the XStream computational resource, supported by the National Science Foundation Major Research Instrumentation program (ACI-1429830). The authors thank Adam H. Steeves for providing a critical reading of the manuscript.

## References

- 1 S. Curtarolo, W. Setyawan, G. L. Hart, M. Jahnatek, R. V. Chepulskii, R. H. Taylor, S. Wang, J. Xue, K. Yang and O. Levy, AFLOW: An Automatic Framework for High-Throughput Materials Discovery, *Comput. Mater. Sci.*, 2012, **58**, 218–226.
- 2 S. P. Ong, W. D. Richards, A. Jain, G. Hautier, M. Kocher, S. Cholia, D. Gunter, V. L. Chevrier, K. A. Persson and G. Ceder, Python Materials Genomics (Pymatgen): A Robust, Open-Source Python Library for Materials Analysis, *Comput. Mater. Sci.*, 2013, **68**, 314–319.
- 3 E. I. Ioannidis, T. Z. H. Gani and H. J. Kulik, molSimplify: A Toolkit for Automating Discovery in Inorganic Chemistry, *J. Comput. Chem.*, 2016, **37**, 2106–2117.
- 4 A. Nandy, C. Duan, J. P. Janet, S. Gugler and H. J. Kulik, Strategies and Software for Machine Learning Accelerated Discovery in Transition Metal Chemistry, *Ind. Eng. Chem. Res.*, 2018, **57**, 13973–13986.
- 5 N. M. O'Boyle, M. Banck, C. A. James, C. Morley, T. Vandermeersch and G. R. Hutchison, Open Babel: An Open Chemical Toolbox, *J. Phys. Chem. Lett.*, 2011, **3**, 33.
- 6 T. J. Martínez, Ab Initio Reactive Computer Aided Molecular Design, *Acc. Chem. Res.*, 2017, **50**, 652–656.
- 7 S. Lubner, Recent Progress in Computational Exploration and Design of Functional Materials, *Comput. Mater. Sci.*, 2019, **161**, 127–134.
- 8 J. Caruthers, J. A. Lauterbach, K. Thomson, V. Venkatasubramanian, C. Snively, A. Bhan, S. Katare and G. Oskarsdottir, Catalyst Design: Knowledge Extraction from High-Throughput Experimentation, *J. Catal.*, 2003, **216**, 98–109.
- 9 S. Katare, J. M. Caruthers, W. N. Delgass and V. Venkatasubramanian, An Intelligent System for Reaction Kinetic Modeling and Catalyst Design, *Ind. Eng. Chem. Res.*, 2004, **43**, 3484–3512.
- 10 A. Corma, M. J. Díaz-Cabanas, M. Moliner and C. Martínez, Discovery of a New Catalytically Active and Selective Zeolite (ITQ-30) by High-Throughput Synthesis Techniques, *J. Catal.*, 2006, **241**, 312–318.
- 11 Y. Zhuo, A. Mansouri Tehrani and J. Brgoch, Predicting the Band Gaps of Inorganic Solids by Machine Learning, *J. Phys. Chem. Lett.*, 2018, **9**, 1668–1673.
- 12 S. De, A. P. Bartok, G. Csanyi and M. Ceriotti, Comparing Molecules and Solids across Structural and Alchemical Space, *Phys. Chem. Chem. Phys.*, 2016, **18**, 13754–13769.
- 13 L. Ward, A. Agrawal, A. Choudhary and C. Wolverton, A General-Purpose Machine Learning Framework for Predicting Properties of Inorganic Materials, *npj Comput. Mater.*, 2016, **2**, 16028.
- 14 G. Pilania, C. Wang, X. Jiang, S. Rajasekaran and R. Ramprasad, Accelerating Materials Property Predictions Using Machine Learning, *Sci. Rep.*, 2013, **3**, 2810.
- 15 B. Meyer, B. Sawatlon, S. Heinen, O. A. von Lilienfeld and C. Corminboeuf, Machine Learning Meets Volcano Plots: Computational Discovery of Cross-Coupling Catalysts, *Chem. Sci.*, 2018, **9**, 7069–7077.
- 16 X. Ma, Z. Li, L. E. K. Achenie and H. Xin, Machine-Learning-Augmented Chemisorption Model for CO<sub>2</sub> Electroreduction Catalyst Screening, *J. Phys. Chem. Lett.*, 2015, **6**, 3528–3533.
- 17 J. P. Janet and H. J. Kulik, Predicting Electronic Structure Properties of Transition Metal Complexes with Neural Networks, *Chem. Sci.*, 2017, **8**, 5137–5152.
- 18 Z. Li, N. Omidvar, W. S. Chin, E. Robb, A. Morris, L. Achenie and H. Xin, Machine-Learning Energy Gaps of Porphyrins with Molecular Graph Representations, *J. Phys. Chem. A*, 2018, **122**, 4571–4578.
- 19 K. Yao, J. E. Herr, D. W. Toth, R. Mckintyre and J. Parkhill, The Tensormol-0.1 Model Chemistry: A Neural Network Augmented with Long-Range Physics, *Chem. Sci.*, 2018, **9**, 2261–2269.
- 20 J. Behler, Perspective: Machine Learning Potentials for Atomistic Simulations, *J. Chem. Phys.*, 2016, **145**, 170901.
- 21 J. S. Smith, O. Isayev and A. E. Roitberg, ANI-1: An Extensible Neural Network Potential with DFT Accuracy at Force Field Computational Cost, *Chem. Sci.*, 2017, **8**, 3192–3203.
- 22 L. Zhang, J. Han, H. Wang, R. Car and E. Weinan, Deep Potential Molecular Dynamics: A Scalable Model with the Accuracy of Quantum Mechanics, *Phys. Rev. Lett.*, 2018, **120**, 143001.
- 23 S. Chmiela, A. Tkatchenko, H. E. Sauceda, I. Poltavsky, K. T. Schütt and K.-R. Müller, Machine Learning of Accurate Energy-Conserving Molecular Force Fields, *Sci. Adv.*, 2017, **3**, e1603015.
- 24 F. A. Faber, L. Hutchison, B. Huang, J. Gilmer, S. S. Schoenholz, G. E. Dahl, O. Vinyals, S. Kearnes, P. F. Riley and O. A. Von Lilienfeld, Prediction Errors of Molecular Machine Learning Models Lower Than Hybrid DFT Error, *J. Chem. Theory Comput.*, 2017, **13**, 5255–5264.
- 25 B. R. Goldsmith, J. Esterhuizen, J. X. Liu, C. J. Bartel and C. Sutton, Machine Learning for Heterogeneous Catalyst Design and Discovery, *AIChE J.*, 2018, **64**, 2311–2323.
- 26 J. R. Kitchin, Machine Learning in Catalysis, *Nat. Catal.*, 2018, **1**, 230.
- 27 J. P. Janet, L. Chan and H. J. Kulik, Accelerating Chemical Discovery with Machine Learning: Simulated Evolution of Spin Crossover Complexes with an Artificial Neural Network, *J. Phys. Chem. Lett.*, 2018, **9**, 1064–1071.



- 28 J. P. Janet, F. Liu, A. Nandy, C. Duan, T. Yang, S. Lin and H. J. Kulik, Designing in the Face of Uncertainty: Exploiting Electronic Structure and Machine Learning Models for Discovery in Inorganic Chemistry, *Inorg. Chem.*, 2019, DOI: 10.1021/acs.inorgchem.9b00109.
- 29 S. Lu, Q. Zhou, Y. Ouyang, Y. Guo, Q. Li and J. Wang, Accelerated Discovery of Stable Lead-Free Hybrid Organic-Inorganic Perovskites via Machine Learning, *Nat. Commun.*, 2018, 9, 3405.
- 30 R. Yuan, Z. Liu, P. V. Balachandran, D. Xue, Y. Zhou, X. Ding, J. Sun, D. Xue and T. Lookman, Accelerated Discovery of Large Electrostrains in BaTiO<sub>3</sub>-Based Piezoelectrics Using Active Learning, *Adv. Mater.*, 2018, 30, 1702884.
- 31 B. Meredig, E. Antono, C. Church, M. Hutchinson, J. Ling, S. Paradiso, B. Blaiszik, I. Foster, B. Gibbons and J. Hattrick-Simpers, Can Machine Learning Identify the Next High-Temperature Superconductor? Examining Extrapolation Performance for Materials Discovery, *Mol. Syst. Des. Eng.*, 2018, 3, 819–825.
- 32 F. Ren, L. Ward, T. Williams, K. J. Laws, C. Wolverton, J. Hattrick-Simpers and A. Mehta, Accelerated Discovery of Metallic Glasses through Iteration of Machine Learning and High-Throughput Experiments, *Sci. Adv.*, 2018, 4, eaaq1566.
- 33 B. Sanchez-Lengeling and A. Aspuru-Guzik, Inverse Molecular Design Using Machine Learning: Generative Models for Matter Engineering, *Science*, 2018, 361, 360.
- 34 Q. Zhao and H. J. Kulik, Where Does the Density Localize in the Solid State? Divergent Behavior for Hybrids and DFT +U, *J. Chem. Theory Comput.*, 2018, 14, 670–683.
- 35 K. D. Vogiatzis, M. V. Polynski, J. K. Kirkland, J. Townsend, A. Hashemi, C. Liu and E. A. Pidko, Computational Approach to Molecular Catalysis by 3d Transition Metals: Challenges and Opportunities, *Chem. Rev.*, 2018, 119, 2453–2523.
- 36 L. Grajciar, C. J. Heard, A. A. Bondarenko, M. V. Polynski, J. Meeprasert, E. A. Pidko and P. Nachtigall, Towards Operando Computational Modeling in Heterogeneous Catalysis, *Chem. Soc. Rev.*, 2018, 47, 8307–8348.
- 37 P. B. Arockiam, C. Bruneau and P. H. Dixneuf, Ruthenium(II)-Catalyzed C-H Bond Activation and Functionalization, *Chem. Rev.*, 2012, 112, 5879–5918.
- 38 C. K. Prier, D. A. Rankic and D. W. C. MacMillan, Visible Light Photoredox Catalysis with Transition Metal Complexes: Applications in Organic Synthesis, *Chem. Rev.*, 2013, 113, 5322–5363.
- 39 G. Rouquet and N. Chatani, Catalytic Functionalization of C(sp<sup>2</sup>)-H and C(sp<sup>3</sup>)-H Bonds by Using Bidentate Directing Groups, *Angew. Chem., Int. Ed.*, 2013, 52, 11726–11743.
- 40 D. M. Schultz and T. P. Yoon, Solar Synthesis: Prospects in Visible Light Photocatalysis, *Science*, 2014, 343, 1239176.
- 41 D. W. Shaffer, I. Bhowmick, A. L. Rheingold, C. Tsay, B. N. Livesay, M. P. Shores and J. Y. Yang, Spin-State Diversity in a Series of Co(II) PNP Pincer Bromide Complexes, *Dalton Trans.*, 2016, 45, 17910–17917.
- 42 C. Tsay and J. Y. Yang, Electrocatalytic Hydrogen Evolution under Acidic Aqueous Conditions and Mechanistic Studies of a Highly Stable Molecular Catalyst, *J. Am. Chem. Soc.*, 2016, 138, 14174–14177.
- 43 M. Schilling, G. R. Patzke, J. Hutter and S. Luber, Computational Investigation and Design of Cobalt Aqua Complexes for Homogeneous Water Oxidation, *J. Phys. Chem. C*, 2016, 120, 7966–7975.
- 44 D. C. Ashley and E. Jakubikova, Ironing out the Photochemical and Spin-Crossover Behavior of Fe(II) Coordination Compounds with Computational Chemistry, *Coord. Chem. Rev.*, 2017, 337, 97–111.
- 45 D. N. Bowman, A. Bondarev, S. Mukherjee and E. Jakubikova, Tuning the Electronic Structure of Fe(II) Polypyridines via Donor Atom and Ligand Scaffold Modifications: A Computational Study, *Inorg. Chem.*, 2015, 54, 8786–8793.
- 46 A. Yella, H. W. Lee, H. N. Tsao, C. Y. Yi, A. K. Chandiran, M. K. Nazeeruddin, E. W. G. Diau, C. Y. Yeh, S. M. Zakeeruddin and M. Gratzel, Porphyrin-Sensitized Solar Cells with Cobalt (II/III)-Based Redox Electrolyte Exceed 12 Percent Efficiency, *Science*, 2011, 334, 629–634.
- 47 R. Czerwieniec, J. B. Yu and H. Yersin, Blue-Light Emission of Cu(I) Complexes and Singlet Harvesting, *Inorg. Chem.*, 2011, 50, 8293–8301.
- 48 F. B. Dias, K. N. Bourdakos, V. Jankus, K. C. Moss, K. T. Kamtekar, V. Bhalla, J. Santos, M. R. Bryce and A. P. Monkman, Triplet Harvesting with 100% Efficiency by Way of Thermally Activated Delayed Fluorescence in Charge Transfer OLED Emitters, *Adv. Mater.*, 2013, 25, 3707–3714.
- 49 P. S. Kuttipillai, Y. M. Zhao, C. J. Traverse, R. J. Staples, B. G. Levine and R. R. Lunt, Phosphorescent Nanocluster Light-Emitting Diodes, *Adv. Mater.*, 2016, 28, 320–326.
- 50 M. J. Leidl, F. R. Kuchle, H. A. Mayer, L. Wesemann and H. Yersin, Brightly Blue and Green Emitting Cu(I) Dimers for Singlet Harvesting in Oleds, *J. Phys. Chem. A*, 2013, 117, 11823–11836.
- 51 C. L. Linfoot, M. J. Leidl, P. Richardson, A. F. Rausch, O. Chepelin, F. J. White, H. Yersin and N. Robertson, Thermally Activated Delayed Fluorescence (TADF) and Enhancing Photoluminescence Quantum Yields of Cu(I)(Diimine)(Diphosphine)(+) Complexes-Photophysical, Structural, and Computational Studies, *Inorg. Chem.*, 2014, 53, 10854–10861.
- 52 D. M. Zink, M. Bachle, T. Baumann, M. Nieger, M. Kuhn, C. Wang, W. Klopper, U. Monkowius, T. Hofbeck, H. Yersin and S. Brase, Synthesis, Structure, and Characterization of Dinuclear Copper(I) Halide Complexes with PAN Ligands Featuring Exciting Photoluminescence Properties, *Inorg. Chem.*, 2013, 52, 2292–2305.
- 53 Y. Minenkov, D. I. Sharapa and L. Cavallo, Application of Semiempirical Methods to Transition Metal Complexes: Fast Results but Hard-to-Predict Accuracy, *J. Chem. Theory Comput.*, 2018, 14, 3428–3439.
- 54 R. J. Deeth, The Ligand Field Molecular Mechanics Model and the Stereoelectronic Effects of d and s Electrons, *Coord. Chem. Rev.*, 2001, 212, 11–34.





- 86 A. Gaulton, A. Hersey, M. Nowotka, A. P. Bento, J. Chambers, D. Mendez, P. Mutowo, F. Atkinson, L. J. Bellis, E. Cibrián-Uhalte, M. Davies, N. Dedman, A. Karlsson, M. P. Magariños, J. P. Overington, G. Papadatos, I. Smit and A. R. Leach, The ChEMBL Database in 2017, *Nucleic Acids Res.*, 2017, **45**, D945–D954.
- 87 P. F. Bernath and S. McLeod, Diref, a Database of References Associated with the Spectra of Diatomic Molecules, *J. Mol. Spectrosc.*, 2001, **207**, 287.
- 88 N. M. O'Boyle, C. Morley and G. R. Hutchison, Pybel: A Python Wrapper for the Openbabel Cheminformatics Toolkit, *Chem. Cent. J.*, 2008, **2**, 5.
- 89 B. Pritchard and J. Autschbach, Theoretical Investigation of Paramagnetic NMR Shifts in Transition Metal Acetylacetonato Complexes: Analysis of Signs, Magnitudes, and the Role of the Covalency of Ligand–Metal Bonding, *Inorg. Chem.*, 2012, **51**, 8340–8351.
- 90 I. S. Ufimtsev and T. J. Martinez, Quantum Chemistry on Graphical Processing Units. 3. Analytical Energy Gradients, Geometry Optimization, and First Principles Molecular Dynamics, *J. Chem. Theory Comput.*, 2009, **5**, 2619–2628.
- 91 P. J. Stephens, F. J. Devlin, C. F. Chabalowski and M. J. Frisch, Ab Initio Calculation of Vibrational Absorption and Circular Dichroism Spectra Using Density Functional Force Fields, *J. Phys. Chem.*, 1994, **98**, 11623–11627.
- 92 A. D. Becke, Density-Functional Thermochemistry. III. The Role of Exact Exchange, *J. Chem. Phys.*, 1993, **98**, 5648–5652.
- 93 C. Lee, W. Yang and R. G. Parr, Development of the Colle-Salvetti Correlation-Energy Formula into a Functional of the Electron Density, *Phys. Rev. B: Condens. Matter Mater. Phys.*, 1988, **37**, 785–789.
- 94 S. H. Vosko, L. Wilk and M. Nusair, Accurate Spin-Dependent Electron Liquid Correlation Energies for Local Spin Density Calculations: A Critical Analysis, *Can. J. Phys.*, 1980, **58**, 1200–1211.
- 95 P. J. Hay and W. R. Wadt, Ab Initio Effective Core Potentials for Molecular Calculations. Potentials for the Transition Metal Atoms Sc to Hg, *J. Chem. Phys.*, 1985, **82**, 270–283.
- 96 J. P. Janet, T. Z. H. Gani, A. H. Steeves, E. I. Ioannidis and H. J. Kulik, Leveraging Cheminformatics Strategies for Inorganic Discovery: Application to Redox Potential Design, *Ind. Eng. Chem. Res.*, 2017, **56**, 4898–4910.
- 97 S. R. Mortensen and K. P. Kepp, Spin Propensities of Octahedral Complexes from Density Functional Theory, *J. Phys. Chem. A*, 2015, **119**, 4041–4050.
- 98 V. R. Saunders and I. H. Hillier, Level-Shifting Method for Converging Closed Shell Hartree-Fock Wave-Functions, *Int. J. Quantum Chem.*, 1973, **7**, 699–705.
- 99 L.-P. Wang and C. Song, Geometry Optimization Made Simple with Translation and Rotation Coordinates, *J. Chem. Phys.*, 2016, **144**, 214108.
- 100 T. Z. H. Gani and H. J. Kulik, Unifying Exchange Sensitivity in Transition Metal Spin-State Ordering and Catalysis through Bond Valence Metrics, *J. Chem. Theory Comput.*, 2017, **13**, 5443–5457.
- 101 E. I. Ioannidis and H. J. Kulik, Towards Quantifying the Role of Exact Exchange in Predictions of Transition Metal Complex Properties, *J. Chem. Phys.*, 2015, **143**, 034104.
- 102 E. I. Ioannidis and H. J. Kulik, Ligand-Field-Dependent Behavior of Meta-GGA Exchange in Transition-Metal Complex Spin-State Ordering, *J. Phys. Chem. A*, 2017, **121**, 874–884.
- 103 H. J. Kulik, M. Cococcioni, D. A. Scherlis and N. Marzari, Density Functional Theory in Transition-Metal Chemistry: A Self-Consistent Hubbard U Approach, *Phys. Rev. Lett.*, 2006, **97**, 103001.
- 104 G. Ganzenmüller, N. Berkaïne, A. Fouqueau, M. E. Casida and M. Reiher, Comparison of Density Functionals for Differences between the High- (T<sub>2g</sub><sup>5</sup>) and Low- (A<sub>1g</sub><sup>1</sup>) Spin States of Iron(II) Compounds. IV. Results for the Ferrous Complexes [Fe(L)(‘NHS<sup>4</sup>’)], *J. Chem. Phys.*, 2005, **122**, 234321.
- 105 A. Droghetti, D. Alfè and S. Sanvito, Assessment of Density Functional Theory for Iron (II) Molecules across the Spin-Crossover Transition, *J. Chem. Phys.*, 2012, **137**, 124303.
- 106 P. Verma, Z. Varga, J. E. Klein, C. J. Cramer, L. Que and D. G. Truhlar, Assessment of Electronic Structure Methods for the Determination of the Ground Spin States of Fe (II), Fe (III) and Fe (IV) Complexes, *Phys. Chem. Chem. Phys.*, 2017, **19**, 13049–13069.
- 107 L. Wilbraham, P. Verma, D. G. Truhlar, L. Gagliardi and I. Ciofini, Multiconfiguration Pair-Density Functional Theory Predicts Spin-State Ordering in Iron Complexes with the Same Accuracy as Complete Active Space Second-Order Perturbation Theory at a Significantly Reduced Computational Cost, *J. Phys. Chem. Lett.*, 2017, **8**, 2026–2030.
- 108 Q. M. Phung, M. Feldt, J. N. Harvey and K. Pierloot, Toward Highly Accurate Spin State Energetics in First-Row Transition Metal Complexes: A Combined CASPT2/Cc Approach, *J. Chem. Theory Comput.*, 2018, **14**, 2446–2455.
- 109 C. Zhou, L. Gagliardi and D. G. Truhlar, Multiconfiguration Pair-Density Functional Theory for Iron Porphyrin with CAS, RAS, and DMRG Active Spaces, *J. Phys. Chem. A*, 2019, **123**, 3389–3394.
- 110 M. C. Kim, E. Sim and K. Burke, Communication: Avoiding Unbound Anions in Density Functional Calculations, *J. Chem. Phys.*, 2011, **134**, 171103.
- 111 F. Jensen, Describing Anions by Density Functional Theory: Fractional Electron Affinity, *J. Chem. Theory Comput.*, 2010, **6**, 2726–2735.
- 112 J. P. Janet, C. Duan, T. Yang, A. Nandy and H. J. Kulik, A Quantitative Uncertainty Metric Controls Error in Neural Network-Driven Chemical Discovery, chemrxiv, DOI: 10.26434/chemrxiv.7900277.v2, 2019.
- 113 C. R. Groom, I. J. Bruno, M. P. Lightfoot and S. C. Ward, The Cambridge Structural Database, *Acta Crystallogr., Sect. B: Struct. Sci., Cryst. Eng. Mater.*, 2016, **72**, 171–179.

